Last improvements in the analysis of resonant strip sensors

Bernard Dulmet and Pierre Tinguy
FEMTO-ST, Dpt CEP
ENSMM, 26 chemin de l'Epitaphe, Besançon FR
Email: bdulmet@ens2m.fr

Yuliyan Lazarov and Lozan Spassov
ISSP-BAS, AELab
72 Tzarigradsko Chaussee blvd, SOFIA BG
Email: julian@issp.bas.bg

***Abstract*— The paper proposes new improvements to a previously established two–dimensional model of $29.3\ MHz$ NLC-cut strip resonators used as temperature sensors. Starting from that previous model, we present a model which takes into account the dependence of the vibration mode along the third coordinate *i.e.* along the length of the strip, by means of Hamilton's principle. Thereafter, an estimation of the C_1 parameter is numerically achieved by performing additional simplifications, which have little effect onto the accuracy in the circumstance. We also present the results of a force–sensitivity experiment applying a compressive load equal to $-1N$ at the end of the sensor narrow plate. The measured frequency shift was close to $1.3\ kHz$. Simple calculations show that the frequency shift predicted by the acousto–elastic effect is much larger than the shift arising from the action of rigid stiffening onto the flexural branch coupled with thickness shear. These first investigations indicate that the force–frequency effect in strip resonators seems to be large enough to make them usable as force sensors.**

I. Introduction

To complement FEA in the development of new miniature sensors based on quartz strip resonators, which compare favorably with traditional platinum gauges [1], we have previously established a two dimensional model based on the use of Hamilton's principle [5] to rule the balancing between contributing branches of the dispersion curves. In a recent paper [2], we discussed several possibilities to extend that model in three dimensions.

This paper shows how such an extension can be achieved by matching approximations of the resonant modes in both the electroded and unelectroded regions at the surface of discontinuity with help of Hamilton's prnciple while free boundary conditions are imposed at both ends of strip. The general approach is similar in scope to the one of Ref. [3], the main difference being that our model is built on combinations of guided waves only instead of Mindlin's method.

Although the theoretical analysis was completed, the details of the accompanying numerical program were not fully consolidated at the time of the conference. Nevertheless, by adding additional simplifying assumptions, we can perform an approximate determination of the motional capacitance of the strip sensors with a fair agreement with data known from experiences.

After a short discussion about the thermal sensitivity, which was previously determined by a FEA program compliant with lagrangian formalism, we essentially focus onto the force sensitivity of the strip resonators, which was previously a completely undocumented subject. Both kinds of sensitivities depend on the aspect ratio of the resonator, which governs the balance between thickness shear and other branches contributing to the structure of the resonant modes, because the separate branches themselves exhibit very different sensitivities. In particular, one would expect that the flexural branch be more affected by environmental parameters than the thickness–shear branch, an idea that could be misleading.

Finally, we present the conditions of a force–frequency experiment which was performed on temperature strip sensors in NLC–cut [6] operating at $29.3\ MHz$. A compressive load of $-1\ N$ was exerted at the ends of strip, which has a cross–section $0.084 \times 2\ mm$. A basic analysis of the obtained frequency shift indicates a combined action of acousto–elastic effect and of the rigid stiffening encounterd in flexural bars used as sensing elements in most of micromachined resonant force sensors.

II. Vibration model

An idealized strip resonator configuration is represented on Fig. 1. L denotes the length of the plate along local x_3 axis of singly rotated $Y+\theta$ cut, $2b$ denotes the length of the electrodes, which cover the whole width w of the plate, and $2h$ denotes the thickness.

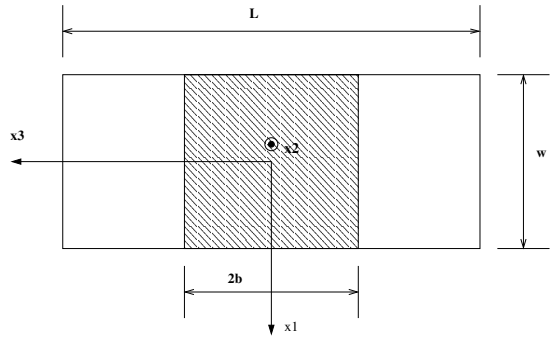

Fig. 1. Basic configuration of strip resonator

A. Simplified initial 2D model

Although a more detailed 2–D model was previously presented [1], in the present paper, we apply more restrictive

simplifying assumptions, actually identical to the ones of Ref. [3]. Neglecting $c_{14},\ c_{24}\ c_{34}, c_{56}$ elastic constants, one obtains

$$\begin{aligned} T_{11} &= c_{11}u_{1,1} + c_{12}u_{2,2} \\ T_{22} &= c_{12}u_{1,1} + c_{22}u_{2,2} \\ T_{12} &= c_{66}\left(u_{1,2} + u_{2,1}\right) \end{aligned} \tag{1}$$

in the cross–section of strip, as far as $\partial/\partial x_3 = 0$. As a consequence, u_3 is neglected, and this simplification will hold in the rest of the analysis. In agreement with above constitutive equations, the two–dimensionnal balance equations expressing Newton's law are :

$$\begin{aligned} c_{11}u_{1,11} + \left(c_{12} + c_{66}\right)u_{2,12} + c_{66}u_{1,22} &= \rho\ddot{u}_1 \\ c_{66}u_{2,11} + \left(c_{12} + c_{66}\right)u_{1,12} + c_{22}u_{2,22} &= \rho\ddot{u}_2 \end{aligned} \tag{2}$$

Then, the most basic boundary conditions to obey are

$$T_{12} = 0 \qquad \text{and} \quad T_{22} = 0 \qquad \text{at} \qquad x_2 = \pm h \tag{3}$$

and this kernel part of the model is solved by the following system of solutions, with symmetry properties pertinent for the analysis of x_1–symmetric modes of the strip resonator :

$$\begin{aligned} u_1 &= \cos\left(\xi x_1\right)\sum_{n=1}^{2} C_n\beta_1^n \sin\left(\eta_n x_2\right) \\ u_2 &= \sin\left(\xi x_1\right)\sum_{n=1}^{2} C_n\beta_2^n \cos\left(\eta_n x_2\right) \end{aligned} \tag{4}$$

From that, the dispersion curves of Fig. 2 are readily obtained. The vertical axis represents the dimensionless angular frequency Ω, obtained after normalization w.r.t. the angular frequency of pure thickness modes in an infinite plate, whereas the horizontal axis is the normalized lateral wavenumber [2]. The lower curve on the figure represents the flexure branch, whereas the upper curve is the fundamental pure thickness–shear branch, B–mode in NLC–cut. The two roots $\eta(\Omega, \gamma)$ of the determinantal equation obtained by substituting (4) into (2) are complex conjugate in the region below the $\Omega = 0.8834\gamma$ straight line, for NLC–cut. The slope can easily be determined analytically. Then, free boundary conditions on the lateral edges of resonator located at $x_1 = \pm w/2$ can be turned into integral conditions by means of the strong form of the variational principle [1], [5]. To satisfy the integral conditions, combinations of branches are needed :

$$\begin{aligned} u_1 &= \sum_{p=1}^{2}\cos\left(\xi_p x_1\right)\sum_{n=1}^{2} C_{(p,n)}\beta_1^{(p,n)} \sin\left(\eta_n^p x_2\right) \\ u_2 &= \sum_{p=1}^{2}\sin\left(\xi_p x_1\right)\sum_{n=1}^{2} C_{(p,n)}\beta_2^{(p,n)} \cos\left(\eta_n^p x_2\right) \end{aligned} \tag{5}$$

With the present assumptions, only the two above–mentionned branches are required, whereas in the rigorous treatment, we would use at least three branches. Then, ω and the distribution of mechanical displacement can be determined in the cross–section of strip. For $w/(2h) = 24.5$, we quickly obtain the distribution of u_1 along x_1 represented on Fig. 3.

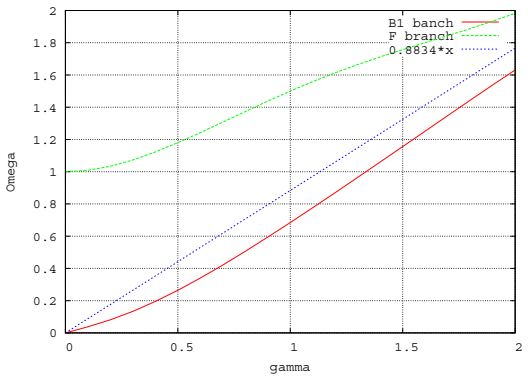

Fig. 2. Dispersion curves in the simplified 2-D model for NLC–cut

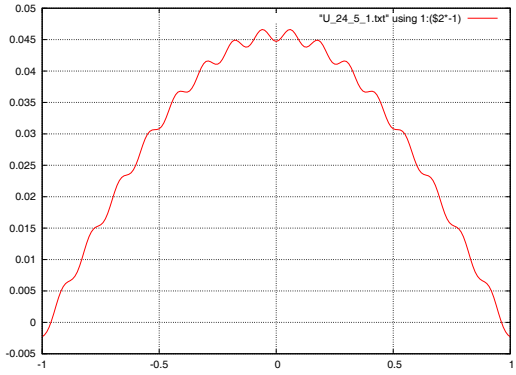

Fig. 3. Distribution of u_1 across the width of plate in the simplified 2-D model for NLC–cut

B. 3D extension by mode matching

Although the theoretical background of the present paper is different form [3], we propose to follow similar steps in the building of the model. We assume that acceptable 3–D solutions have the form :

$$\begin{aligned} u_1(x_1, x_2, x_3) &= \bar{u}_1(x_1, x_2)\hat{u}_1(x_3) \\ u_2(x_1, x_2, x_3) &= \bar{u}_2(x_1, x_2)\hat{u}_2(x_3) \end{aligned} \tag{6}$$

where $\bar{u}_1$ and $\bar{u}_2$ are exactly the displacement distributions obtained in the previously 2-D treatment, while the constitutive equations to be considered in the 3-D model are the following :

$$\begin{aligned} T_{11} &= c_{11}u_{1,1} + c_{12}u_{2,2} \\ T_{22} &= c_{12}u_{1,1} + c_{22}u_{2,2} \\ T_{12} &= c_{66}\left(u_{1,2} + u_{2,1}\right) \\ T_{23} &= c_{44}u_{2,3} \\ T_{31} &= c_{55}u_{1,3} \end{aligned} \tag{7}$$

and the 3–D propagation equations are :

$$\begin{aligned} c_{11}u_{1,11} + \left(c_{12} + c_{66}\right)u_{2,12} + c_{66}u_{1,22} + c_{55}u_{1,33} &= \rho\ddot{u}_1 \\ c_{66}u_{2,11} + \left(c_{12} + c_{66}\right)u_{1,12} + c_{22}u_{2,22} + c_{44}u_{2,33} &= \rho\ddot{u}_2 \end{aligned} \tag{8}$$

Such a simplified 3–D is accurate only if u_3 is actually very small, nevertheless it is altogether invaluable as a way to structure our analytical understanding of the strip resonator. It does not make much of a problem since extensive FEA simulations and X-rays topography have been already performed on those temperature sensors [1]. Correction terms can be introduced into above equations to account for mass–loading and electrode-shortening effects in the electroded region as well as piezoelectic stiffening along the thickness in both electroded and unelectroded regions. Thus, slightly different displacement distributions and values of ω are obtained in the electroded and unelectroded regions, which we symbolically denote by e and u. Nevertheless, Tiersten's book [7] provides with a strong form of Hamilton's principle appropriate to treat the case of internal surfaces of discontinuity. In the present case, it takes the following form :

$$\begin{aligned}
&\int_{V_{e\&u}} \left\{ \left[T_{11,1} + T_{12,2} + T_{31,3} + \rho\omega^2 u_1 \right] \delta u_1 \right. \\
&\left. + \left[T_{12,1} + T_{22,2} + T_{32,3} + \rho\omega^2 u_2 \right] \delta u_2 \right\} dV_{e\&u} \\
&+ \int_{S_d} \frac{1}{2} \left[c_{55} \left(u_{1,3}^+ - u_{1,3}^- \right) \left(\delta u_1^+ + \delta u_1^- \right) \right. \\
&\qquad \left. + c_{44} \left(u_{2,3}^+ - u_{2,3}^- \right) \left(\delta u_2^+ + \delta u_2^- \right) \right] dS_d \qquad (9) \\
&+ \int_{S_d} \frac{1}{2} \left[\left(u_1^- - u_1^+ \right) c_{55} \left(\delta u_{1,3}^+ + \delta u_{1,3}^- \right) \right. \\
&\qquad \left. + \left(u_2^+ - u_2^- \right) c_{44} \left(\delta u_{2,3}^+ + \delta u_{2,3}^- \right) \right] dS_d \\
&- \int_{S_f} \left[c_{55} u_{1,3} \delta u_1 + c_{44} u_{2,3} \delta u_2 \right] dS_f = 0
\end{aligned}$$

Here, S_d denotes the surface of discontinuity between electroded and unelectroded regions, S_f represents the x_3-oriented stress–free surfaces at both ends of strip, and we use the symbolic notation $V_{e\&u}$ to indicate that the volume integral should be separately performed in the electroded and unelectroded regions with the 2D solutions $\bar{u}_1(x_1, x_2)$ and $\bar{u}_2(x_1, x_2)$ for each region. Quantities with superscript "+" are taken on the positive side of the unit normal of the interface, for instance the unelectroded region if one looks at the $x_3 > 0$ electrode end, and of course the quantites with "-" are evaluated at the other side of discontinuity. This writing of the strong form of Hamilton's principle is in conformity with the extension proposed in Tiersten's book, Eq. (6.44) Chap. 6, to take into account internal surfaces of discontinuity. The variations are specified in the following way :

$$\delta u_1 = \bar{u}_1 (x_1, x_2)\, \delta \hat{u}_1(x_3) \quad \delta u_2 = \bar{u}_2 (x_1, x_2)\, \delta \hat{u}_2(x_3) \qquad (10)$$

Taking advantage of (10) and of the considerable part of 3–D equations which is already satisfied by the initial 2–D solutions, it is easily demonstrated that the volume integrals appearing in (9) identically vanish provided that the approximate 3–D solutions (6) satisfy the following system :

$$\begin{aligned}
&\int_{-h}^{+h} \int_{-\frac{w}{2}}^{\frac{w}{2}} \left[\rho \left(\omega^2 - \omega_{e\&u}^2 \right) \bar{u}_1 \bar{u}_1 - (c_{12} + c_{66})\, \bar{u}_{2,12} \bar{u}_1 \right] dx_2 dx_1 \hat{u}_1 \\
&+ \int_{-h}^{+h} \int_{-\frac{w}{2}}^{\frac{w}{2}} c_{55} \left(\bar{u}_1 \right)^2 dx_2 dx_1 \hat{u}_{1,33} \\
&+ \int_{-h}^{+h} \int_{-\frac{w}{2}}^{\frac{w}{2}} (c_{12} + c_{66})\, \bar{u}_{2,12} \bar{u}_1 dx_2 dx_1 \hat{u}_2 = 0 \\
&\int_{-h}^{+h} \int_{-\frac{w}{2}}^{\frac{w}{2}} \left[\rho \left(\omega^2 - \omega_{e\&u}^2 \right) \bar{u}_2 \bar{u}_2 - (c_{12} + c_{66})\, \bar{u}_{1,12} \bar{u}_2 \right] dx_2 dx_1 \hat{u}_2 \\
&+ \int_{-h}^{+h} \int_{-\frac{w}{2}}^{\frac{w}{2}} (c_{12} + c_{66})\, \bar{u}_{1,12} \bar{u}_2 dx_2 dx_1 \hat{u}_1 \\
&+ \int_{-h}^{+h} \int_{-\frac{w}{2}}^{\frac{w}{2}} c_{44} \left(\bar{u}_2 \right)^2 dx_2 dx_1\ \hat{u}_{2,33} = 0
\end{aligned} \qquad (11)$$

Then, one obtains the following form for the x_3–dependent part in the electroded region :

$$\begin{aligned}
\hat{u}_1^e &= \sum_{n=1}^{2} F_n \mu_1^n \cos \nu_n x_3 \\
\hat{u}_2^e &= \sum_{n=1}^{2} F_n \mu_2^n \cos \nu_n x_3
\end{aligned} \qquad (12)$$

where the two ν_n are obtained as roots of the determinant of the sytem (11) which turns out to be a very simple and common system, if we put aside the detailed form of its coefficients :

$$\begin{bmatrix} d_0 \left(\omega^2 - \omega_{e\&u}^2 \right) - a_1 - a_0 \nu^2 & a_1 \\ a_3 & d_2 \left(\omega^2 - \omega_{e\&u}^2 \right) - a_3 - a_2 \nu^2 \end{bmatrix} \begin{bmatrix} \mu_1 \\ \mu_2 \end{bmatrix} = \begin{bmatrix} 0 \\ 0 \end{bmatrix} \qquad (13)$$

Outside the electrodes, the solution should take a slightly more complicate form :

$$\begin{aligned}
\hat{u}_1^u &= \sum_{n=1}^{2} \chi_1^n \left(H_n \cos \zeta_n x_3 + L_n \sin \zeta_n x_3 \right) \\
\hat{u}_2^u &= \sum_{n=1}^{2} \chi_2^n \left(H_n \cos \zeta_n x_3 + L_n \sin \zeta_n x_3 \right)
\end{aligned} \qquad (14)$$

to permit to impose continuity conditions across the electrode border, located at $x_3 = \pm b$, as well as boundary conditions onto the free edges located at $x_3 = \pm L/2$. The solutions in electroded and unelectroded regions are determined separately. The variations corresponding to the form of the trial functions are the following :

$$\begin{aligned}
\delta \hat{u}_1^e &= \sum_{n=1}^{2} \mu_1^n \cos \nu_n x_3\ \delta F_n \\
\delta \hat{u}_2^e &= \sum_{n=1}^{2} \mu_2^n \cos \nu_n x_3\ \delta F_n
\end{aligned} \qquad (15)$$

in the electroded region, and

$$\begin{aligned}\delta\hat{u}_1^u &= \sum_{n=1}^{2} \chi_1^n \left(\cos\zeta_n x_3\ \delta H_n + \sin\zeta_n x_3\ \delta L_n\right)\\ \delta\hat{u}_2^u &= \sum_{n=1}^{2} \chi_2^n \left(\cos\zeta_n x_3 \delta H_n\ + \sin\zeta_n x_3\ \delta L_n\right)\end{aligned} \tag{16}$$

in the unelectroded region. Because the trial functions have been chosen to cancel the volume integrals, only the terms involving the surface integrals over S_d and S_f remain in the variational principle :

$$\begin{aligned}\int_{S_d} \frac{1}{2}\Big[&c_{55}\left(u_{1,3}^+ - u_{1,3}^-\right)\left(\delta u_1^+ + \delta u_1^-\right)\\ &+c_{44}\left(u_{2,3}^+ - u_{2,3}^-\right)\left(\delta u_2^+ + \delta u_2^-\right)\Big]\ dS_d\\ +\int_{S_d} \frac{1}{2}\Big[&\left(u_1^- - u_1^+\right) c_{55}\left(\delta u_{1,3}^+ + \delta u_{1,3}^-\right)\\ &+\left(u_2^- - u_2^+\right) c_{44}\left(\delta u_{2,3}^+ + \delta u_{2,3}^-\right)\Big]\ dS_d\\ -\int_{S_f} &\left[c_{55} u_{1,3}\delta u_1 + c_{44} u_{2,3}\delta u_2\right]\ dS_f = 0\end{aligned} \tag{17}$$

After performing the following identifications :

$$\begin{aligned}u_1^- - u_1^+ &\equiv \left[\bar{u}_1^e\left(x_1,x_2\right) - \bar{u}_1^u\left(x_1,x_2\right)\right]\hat{u}_1(b)\\ u_2^- - u_2^+ &\equiv \left[\bar{u}_2^e\left(x_1,x_2\right) - \bar{u}_2^u\left(x_1,x_2\right)\right]\hat{u}_3(b)\\ u_{1,3}^+ - u_{1,3}^- &= \bar{u}_1^u\left(x_1,x_2\right)\hat{u}_{1,3}^u(b) - \bar{u}_1^e\left(x_1,x_2\right)\hat{u}_{1,3}^e(b)\\ u_{2,3}^+ - u_{2,3}^- &= \bar{u}_2^u\left(x_1,x_2\right)\hat{u}_{2,3}^u(b) - \bar{u}_2^e\left(x_1,x_2\right)\hat{u}_{2,3}^e(b)\\ u_{1,3}^{\frac{L}{2}} &= \bar{u}_1^u\left(x_1,x_2\right)\hat{u}_{1,3}^u\left(L/2\right)\\ u_{2,3}^{\frac{L}{2}} &= \bar{u}_2^u\left(x_1,x_2\right)\hat{u}_{2,3}^u\left(L/2\right)\end{aligned} \tag{18}$$

and substituting (12,14) and the variations (15,16) into the main system (17), the model is completed from the theoretical point of view. The resonant frequency is obtained by zeroing the determinant of system of coefficients of the F_n, G_n and H_n amplitude constants. Then, every quantity can be determined.

C. Computation of motional capacitance

The motional capacitance can classically be obtained in the framework of the modal discomposition by adding the piezoelectric driving term to the second member of the x_3–dependent sytem :

$$\begin{aligned}\left[-a_1 + d_0\left(\omega^2 - \omega_{e\&u}^2\right)\right]\tilde{u}_1 + a_0\tilde{u}_{1,33} + a_1\hat{u}_2\\ = \rho\omega^2\frac{e_{26}V}{2hc_{66}}\int_{-\frac{w}{2}}^{+\frac{w}{2}}\int_{-h}^{+h} x_2\bar{u}_1\left(x_1,x_2\right)dx_2\\ a_3\hat{u}_1 + \left[-a_3 + d_2\left(\omega^2 - \omega_{e\&u}^2\right)\right]\hat{u}_2 + a_2\hat{u}_{2,33} = 0\end{aligned} \tag{19}$$

This is readily obtained through the usual variable change :

$$\begin{aligned}u_1(x_1,x_2,x_3) &= \bar{u}_1(x_3)\bar{u}_1(x_1,x_2)\\ &= \tilde{u}_1(x_3)\bar{u}_1(x_1,x_2) - \frac{e_{26}V}{2hc_{66}}x_2\end{aligned} \tag{20}$$

which has no effect on the terms in the second line of the system. Then, the computations becomes formally identical to the ones found for instance in [8], [9]. The current is given by the surface integral of the time derivative of electric displacement under the electrode :

$$I = -4\int_0^{\frac{w}{2}}\int_0^b \dot{D}_2\, dx_1 dx_2 \tag{21}$$

In the present case, the modal discomposition has to be limited to a single term, and C_1 can be obtained by identification. Because the numerical program implementing the model was well under way, but not entirely completed at the time of conference[1], we had to perform additional computations to complete an approximate calculation. For that we matched only the essentially TS branches corresponding to ν_1 in (13) across the electrode border, an approach nearly identical to the one which was proposed for simpler calculations[2] in a previous paper [2]. Such calculation estimate the series capacitance with a quite reasonable accuracy : calculated value $C_1 \approx 9.5\ fF$, measured $C_1 \approx 8 - 10\ fF$.

D. Thermal sensitivities

Above–presented model can be rewritten in the framework of the theory previously proposed in [10]. This theory requires a rewriting of the elastic coefficients and, in particular, it breaks the symmetry of usual elastic constants, for instance $c_{1212} \neq c_{2121}$. Nevertheless, once the initial writing is performed, the heory does not increase the degree of the various developments encountered upon building the model. Since the thermal sentivity of the quartz NLC–cut strip sensors was previously investigated [1] and the typical results are solidly known and well controlled, we do not put more focus on this field in the present paper and leave it for further publication.

III. Force–frequency experiments and analysis

The setup used in that experiment consists in four main parts :

- a traction - compression system (DMA 3220 High Resolution + Force sensor 22N - BOSE),
- a network analyzer (Agilent E5100A, 10kHz 300 MHz),
- an electronic interface,
- the strip resonator itself.

The traction–compression system includes a force sensor to easily determine the applied force. This system is fully computer–controlled, within an accuracy of $0.01\ N$. The frequency variations are directly observed with the network analyzer. Although the resonator was electrically connected to the analyzer by a classical four resistors π–network, some conditionning was required before the tests. First, it was necessary to electrically connect the electrodes by two Nickel wires ($\phi\ 140\ \mu m$) mandatorily out of the way of the (conductive) clamps of the traction–compression machine. From another hand, the wires must be welded as far as possible

[1] x_3-dependent sytem working, but the checking of final system over S_d and S_f not completed.

[2] for instance, upon obtaining the Fig. 10 of the quoted paper.

from the center of the resonator in order to minimize the disturbance of the vibration. Then, some insulating mechanical interface was required between the resonator and the iron clamps of the machine. We realized this function through a PVC holder onto which one end of strip resonator was glued with Araldite, chosen for its high mechanical strength. In the compression experiments, the bottom part of the mechanical interface consists of a piece of polymer, rather souple, thereby avoiding to damage the bottom end of the strip, while being altogether resistant.

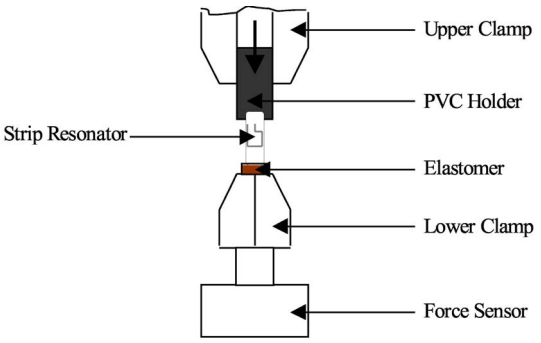

Fig. 4. Mounting of resonator for compressive tests

The flexibility of holding system has little impact on the experiment since the feedback of the traction machine allows for a precise control of the exerted force. Since the sensors provided by ISSP-BAS are thermometers, and it was out of reach to operate a rigorous temperature control in the room where the experiments took place, we had to follow a procedure able to minimize or compensate the influence of the thermal drift. A cycling method solves this issue. Obtained results are given below, in the sequence with which they have been obtained.

Force (N)	Z (Ω)	f (MHz)	δf (Hz)
0	50.6	29.370655954	-
1	50.44	29.369402336	- 62.4
2	50.87	29.368050985	- 1351.351
1	50.62	29.369539732	+ 1488.747
2	50.36	29.368033998	- 1595.734
1	50.81	29.369421504	+ 1387.506
2	50.36	29.368028743	- 1392.761
3	50.17	29.366788700	- 1240.043

The sample broke at the end of experiment when we tried to increase the compressive load up to $-5\ N$. Eliminating the thermal drift (nearly 0.25^oC over the duration of the experiment) by least square method, we obtain a frequency sensitivity of $-1.365\ kHz/N$, which is actually rather large. The system of exerted static stresses is basically one of plane stresses, namely T_{11}, T_{33}, T_{13}. Then, the relative frequency shift predicted by acoustoelastic effect can be roughly estimated by the formula :

$$\frac{\delta\omega}{\omega} \approx \frac{c_{66k}S_k + 2c_{66}S_1}{2c_{66}} \tag{22}$$

Exerting an homogenous compressional stress $T_{33} = F/(2hw)$ along the length of resonator results into a perpendicular extensional stress :

$$T_{11} = -\frac{c_{13} - \dfrac{c_{12}c_{23}}{c_{22}}}{c_{33} - \dfrac{c_{23}^2}{c_{22}}}\, T_{33}, \tag{23}$$

and, finally, we obtain

$$\frac{\delta\omega}{\omega} \approx \frac{(2c_{66} + c_{661})\, s_{13} + c_{662}s_{23} + c_{663}s_{33} + c_{664}s_{34}}{2c_{66}} T_{33}. \tag{24}$$

Substituting the elastic constants of NLC–cut, we obtain the average values $T_{33} \approx -6.1\ MPa$ when a global load $F_z = -1\ N$ is applied to the sample. Then the analysis, entirely based on the evaluation of the action of acoustoelastic effect upon the TS branch, predicts a frequency shift $\delta f = -1997\ Hz$ for $F_z = -1\ N$ in here-described experiment.

From the other hand, one would think that the rigid stiffening effect, close to the stretched string effect, and applied in most vibrating beam force sensors, does impact the force sensitivity of the flexural branch. It can be estimated in the following manner. From the simple stress analysis above, which was onfirmed by a static finite element analysis, one obtains $T_{11} \approx +0.37\ MPa$. Assuming that the (x_3, x_2) cross section remains plane according to Bernoulli's assumption, it can be shown at the textbook level that the frequency of the strip vibrating in flexural modes in the plane (x_1, x_2) is given by the formula :

$$\rho\omega^2 = \beta^2 \left(T_{11} + E_b \frac{h^3}{4}\beta^2 \right) \tag{25}$$

where E_b is the biaxial modulus of the plate, estimated at $79\ 10^9\ Pa$ for here–studied configuration. β is a wavenumber coefficient, which actually depends on T_{11} in usual applications. Nevertheless, for high harmonics of flexure, as is presently the case, this dependence is rather small, so that we can directly identify β from the value of resonant frequency in the absence of stress. Performing this approximation, we have obtained $\delta f \approx +41\ Hz$ for this effect. Thus, although it is not sufficient to improve the accuracy of results predicted by acousto-elastic effect, it adds a correction in the right direction. We initially overestimated the expected value of rigid–stifening effect, but it appears upon closer examination that the effect quickly weakens with the increase of the flexure overtone. Gathering both effects into a single formalism remains to be done. It seems a tricky task, because thickness shear vibrations are consistentlly described in the framework of elasticity, while flexural vibrations can be easily described in the framework of engineering stress analysis, where bending momenta are explicitely considered, whereas they are implicitely taken into account by the symmetry of stresses in the theory of elasticity.

We inted to confirm the results of this first analysis by performing further tests in traction by following the procedure outlined on Fig. 4 in order to eliminate parasitic bendings originated by disalignement between the two PVC holders.

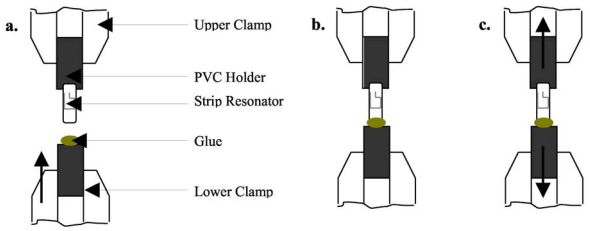

Fig. 5. Mounting of strip resonator for extensional tests

IV. Conclusion

Although we presented it with the same restrictive assumptions as previously proposed in [3], the proposed mode–matching model is not restricted by principle to taking into account only two branches of the dispersion curves. More branches can be incorporated, at the expense of an increased dimension of the determinantal systems together with an increased number of integrals.

Although a detailed analytical study of force–frequency effect in strip resonators would require a more dedicated effort, the experimentally–observed strength of this effect is large enough to consider that strip resonators can be promising for force sensing by high frequency resonators as a whole, if one considers that strip resonators can provide a comparatively better frequency stability than flexural beams.

Acknowledgements

The authors are deeply thankful to Laurent Hirsinger from FEMTO-ST Dpt. of Mechanics, who provided and set up the traction machine used in here–presented force–frequency measurements, while providing useful advices about this experiments. They also thank the french CNRS and the Bulgarian Academy of Sciences for the bilateral support of this cooperation.

References

[1] B. Dulmet, L. Spassov, R. Bourquin, A. Ivan, Ts. Angelov, Yu. Lazarov, *Design of a new miniature resonant temperature sensor in NLC-cut of quartz*, Proc. E.F.T.F., (2005).

[2] B. Dulmet, Yu. Lazarov, L. Spassov, *Semi Analytical Modelling of Thermosensitive Strip Resonators*, Proc. E.F.T.F., (2006).

[3] H.F. Tiersten and T.-L. Sham, *A calculation to the resonant frequencies and motional capacitances for the fundamental family of modes of AT–cut quartz strip resonator* , Proc. IEEE Intl. Freq. Ctrl. Symp., pp 947–955, (1998).

[4] R.D. Mindlin, *High Frequency Vibrations of Crystal Plates, Quarterly of Applied Mathematics*, April 1961, nř1, pp. 51–61(1961).

[5] H.F. Tiersten, *Natural boundary conditions and initial conditions from a modification of Hamilton's principle*, J. Math. Phys., **9**, nř9, pp 1445–1450, Sept. 1968.

[6] L. Spassov, E. Yossiffov, V. Georgiev, L. Vergov, *A rotated Y-cut quartz resonator with a linear temperature-frequency characteristic*, Sensors & Actuators, A58, pp. 185–189, (1997).

[7] H.F. Tiersten, *Linear Piezoelectric Plates vibrations*, Plenum Press, N. Y., (1969).

[8] J.A. Lewis, *The Effect of Driving Electrode Shape on the Electrical Properties of Piezoelectric Crystals*, The Belle System Technical Journal, pp. 1250–1280, Sept. 1961.

[9] H.F. Tiersten, *Analysis of trapped-energy resonators operating in overtones of coupled thickness shear and thickness twist*, J. Acoust. Soc. Am., Vol. 59, N 4, pp. 879–888, April 1976.

[10] B. Dulmet and R. Bourquin, *Lagrangian effective material constants for the modeling of thermal behavior of acoustic waves in piezoelectric crystals. Parts I& II*, J. Acoust. Soc. Am. 110 (4), pp. 1792–1799 and 1800–1807, October 2001.